Journal of Photochemistry and Photobiology A: Chemistry 222 (2011) 56–63

Contents lists available at ScienceDirect

Journal of Photochemistry and Photobiology A: Chemistry

journal homepage: www.elsevier.com/locate/jphotochem

Tuning the formation of aggregates in silica–Rhodamine 6G hybrids by thermal treatment

Carlo M. Carbonaro*

Dipartimento di Fisica, Università di Cagliari, s.p. n°8 Km 0.700 09042 Monserrato (Ca), Italy

ARTICLE INFO

Article history:
Received 25 February 2011
Received in revised form 22 April 2011
Accepted 6 May 2011
Available online 18 May 2011

Keywords:
Aggregates
Organic–inorganic hybrids
Optical spectroscopy
Exciton theory

ABSTRACT

The formation of fluorescent J aggregates in organic–inorganic Rhodamine 6G–silica hybrids is investigated in sol–gel prepared bulk samples in the concentration range of the transition from fluorescent to non-fluorescent aggregates (1.0×10^{-4}–1.0×10^{-3} mol/l). The spectral properties of the observed aggregates are studied by recording the excitation and emission fluorescence spectra and the fluorescence decay kinetics and analyzed in the exciton theory framework. The reported optical features depend both on the synthesis technique and the post synthesis treatments. It is shown that the geometry of fluorescent J aggregates can be modified from oblique to coplanar inclined configuration by thermal treatment of the samples.

1. Introduction

The mild preparation conditions of the sol–gel technique and the endless versatility of the organic chemistry allow to design and develop organic–inorganic hybrids to address specific requirements in numerous technological fields, from the environmental control (e.g. organosilicates for biocatalysis), to the light harvesting (e.g. dye doped TiO_2 in solar cell) or the controlled delivery and release of drugs (e.g. coumarin doped porous silica) [1–3]. The large specific surface of a porous host allows to introduce within its pores a large quantity of the dye molecules of interest to exploit a concentration effect in order to increase, for example, the drug content released by the matrix of a drug delivery system or the harvested energy in a dye-sensitized solar cell [4]. However the limits of this concentration effect depend on the host-guest interaction, also known as "cage-effect": even though the aggregation phenomena are expected to be reduced by the presence of the additional external potential (that is the porous surface) the concentration dependent formation of molecular aggregates can lead, in general, to different chemical–physical properties of the synthesized hybrid and its control represents a challenging goal in the designing and engineering of organic–inorganic hybrids for high-tech applications [5]. Among the possibilities, mesoporous silica doped with fluorescent dyes were largely investigated in the last decades aiming to realize luminescent materials for applications in photonic such as solid state lasers and luminescent devices [6–14].

The introduction of the fluorescent dyes, typically dissolved in alcoholic solutions, into the transparent porous silica matrix can be achieved or by direct impregnation of the sol–gel prepared silica host (post-doping method) or by the so-called "one-pot" synthesis, where the dye molecules are introduced at the sol stage of the sol–gel technique (pre-doping method). In both cases the dye molecules are bonded to the host matrix via electrostatic interactions once the solvent is evaporated and the formed hybrids are classified as type I. With the one-pot synthesis it is also possible to design a specific precursor of the chosen dye molecule to achieve a covalent bond between the guest and the silica matrix. In this case the prepared hybrids are classified as type II [15].

The archetypal dye-doped silica hybrid contains Rhodamine 6G (Rh6G), a well studied Xanthene dye known for its high quantum yield and its laser tunability in the 550–600 nm [16]. The optical performances of Rh6G–silica hybrid [10,17–20] are related to the tendency of Rh6G to form molecular aggregates: if the formation of dimers is reported in concentrated solutions for dye concentration above 10^{-5} mol/l in water and 10^{-2} mol/l in alcohols [21], the adsorption of Rh6G molecules on porous silica surface displays the presence of dimers starting from dye concentration of about 10^{-5} mol/l [10]. Aggregation phenomena were also reported in parent systems where the dye molecules were introduced within layered clays showing the formation of different types of aggregates [22–27]. According to the exciton theory, when the distance between two monomer units is reduced two kinds of dimers can be formed: non-fluorescent H dimers, which show a blue shifted absorption band with respect to the wavelength peak position of the monomer species, and fluorescent J dimers, characterized by a red shifted emission band with respect to the wavelength peak

* Tel.: +39 0706754823; fax: +39 070510171.
E-mail address: cm.carbonaro@dsf.unica.it

1010-6030/$ – see front matter © 2011 Elsevier B.V. All rights reserved.
doi:10.1016/j.jphotochem.2011.05.001

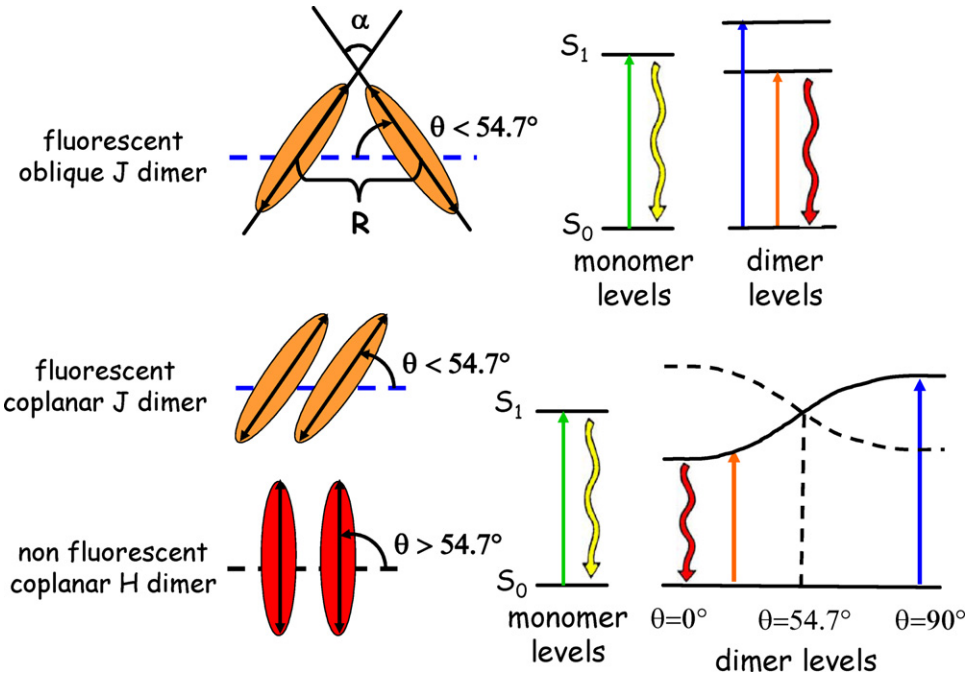

Fig. 1. Schematic picture of geometric arrangements of dimers and their electronic levels.

position of the emission band of the monomers [29,30]. Beside the dye concentration dependence, the formation of fluorescent or non-fluorescent dimers depends on the host-guest interaction, that is the interaction between the dye molecules and the silica surface, which determines the geometry adopted by the two monomers on the surface itself [31–34]. As the dye concentration increases also larger aggregates could be formed, as reported in layered clays or in water solution [35]. In addition the aggregation phenomenon could also depend on the Rh6G counterion, since it was reported that in alcoholic solution chloride Rh6G exhibits a smaller tendency to J dimerization than perchlorate Rh6G [32]. With reference to the scheme reported in Fig. 1, H dimers are characterized by a coplanar sandwich type configuration with an angle between the monomer transition moments and the silica surface larger than 54.7°; J dimers can adopt both a coplanar sandwich configuration or an oblique head-to-tail configuration with the reference angle smaller than 54.7° [29,32]. When the excited state of the monomers is split in two excited states of the dimers, the exciton theory expectation is that oblique J dimers have two allowed singlet–singlet electronic transitions to both the excited states while coplanar J dimers display the transition only to and from the lowest excited state. Conversely, in the case of H dimers the absorption transition from the ground state to the highest excited state is the only allowed transition. The analysis of the optical features of the investigated hybrids allows to discriminate among the different kind of formed aggregates and their effect on the applications in the photonic field: if the presence of H dimers is detrimental for solid state laser devices because of the quenching of the monomer emission, the formation of J dimers could grant different spectral and time tunability to the luminescent hybrid [8–14]. For example, the presence of J aggregates of polymethine dyes was exploited to produce laser active media [36]. It was reported in the literature that Xanthene dyes form oblique J dimers in dye doped sol–gel silica [10] but for Rhodamine 101, where coplanar J dimers were observed because of its molecular structure [11]. In the case of Rhodamine 110 the formation of coplanar J dimers was induced by decreasing the specific porous surface available for the adsorption and keeping constant the concentration [9]. These results indicate the possibility of aggregation tuning by changing the synthesis conditions or applying specific post synthesis treatments. The formation of J dimers was reported in the 10^{-6}–10^{-4} mol/l concentration range, above which the transition from fluorescent to non fluorescent dimers is observed. In a previous paper we reported the formation of fluorescent J aggregates in Rh6G–silica type I hybrids prepared by the pre-doping sol–gel technique [19]. In the present paper we studied the dye aggregation in type I samples prepared with different Rh6G precursors (perchlorate and chloride Rh6G) in the 10^{-4}–10^{-3} mol/l concentration range, that is just within the limit of the transition from J to H dimers, and subjected to a post-synthesis thermal treatment. The aim of the work is to investigate the possibility to control the formation of aggregates in pre-doping type I hybrids realized under different conditions, that is by changing the dye counterion or by applying thermal treatment. The ambitious goal is to achieve the capability to control the aggregation state of Rh6G in dye-doped silica hybrids which is a technological relevant issue for the designing and engineering of devices based on controlled organic–inorganic luminescent hybrids.

2. Materials and methods

Two sets of pre-doping type I organic–inorganic Rh6G–silica bulk samples were investigated (Table 1) with dye concentration ranging between 1.6×10^{-4} and 1.6×10^{-3} mol/l. The two sets of xerogels were synthesized with the perchlorate (labeled with "P") and chloride (labeled with "C") Rh6G laser grade dye (Exciton). Samples were sol–gel synthesized by adding dye molecules at the sol stage, according to the following recipe [17]: 0.125 moles of tetra-ethyl-orthosilicate (TEOS) were added to 50 ml of an aqueous solution of HCl (0.01 N) and mixed with 12.5 ml of ethanol as a co-solvent. The mixture was stirred for 15 min and then ethanol was removed by distillation at 35 °C by a rotating evaporator to obtain 45 ml of sol. Samples with different dye concentration were prepared by adding to the sol the chosen Rhodamine salt dissolved in methanol, together with NH_4OH (0.05 N) to increase pH from 2 to 4.2. Type I sols were poured on suitable molds. Gelation occurred in about 3 days; gels were aged for at least 1 day in the mold, extracted and dried at room conditions for about 1 month. A second set of samples was subjected to thermal

Table 1
Spectroscopic features (λ_{em} = emission peak, FHWM = full width at half maximum, τ = estimated decay time, PL-IA = integrated area of the PL spectrum) of type I Rh6G–silica hybrids excited at 337 nm. "P" and "C" subscripts refer to perchlorate and chloride samples. Data between brackets refer to thermally treated samples. Decay times were estimated through a single exponential fit procedure applied to the PL intensity integrated over the whole spectral range, as described in the text. Estimated uncertainty was less than 0.05 ns. Square correlation factor of the fit procedure $R^2 > 0.96$.

Sample	[Rh6G] (mol/l)	λ_{em}–FWHM (nm)	τ (ns)	PL-IA (arb. units)
A_P	1.6×10^{-4}	552–45 (555–47)	4.69 (4.27)	0.20
B_P	5.2×10^{-4}	559–41 (559–47)	4.75 (4.81)	0.47
C_P	1.0×10^{-3}	559–42 (563–47)	4.67 (4.74)	0.36
D_P	1.6×10^{-3}	565–41 (559–49)	3.49 (4.92)	0.17
A_C	1.6×10^{-4}	554–44 (561–42)	5.14 (5.06)	0.27
B_C	5.2×10^{-4}	558–43 (561–40)	5.21 (4.52)	0.39
C_C	1.0×10^{-3}	562–44 (555–42)	5.93 (5.15)	0.41
D_C	1.6×10^{-3}	562–45 (561–41)	5.22 (4.65)	0.38

treatment with a drying procedure at 65 °C (in this case the samples are labeled with "T"). Prepared samples were bulk disks with diameter of 10 mm and thickness of about 5 mm. The dye distribution is homogeneous, no differences in the spectroscopic features were detected when sampling different points of the same sample. To account for the differences between the initial sol-dilution and the different shrinkage of the wet-gel samples during the drying stage, the Rh6G concentration (mol/l) was calculated on the measured final volume of the xerogel samples. These data could be affected by an error of ±15%. Porosity data were deduced from N_2 adsorption/desorption isotherms (Thermo Electron Sorptomatic 1990) by analyzing adsorption data in the Brunauer, Emmett and Teller (BET) framework and desorption data by means of the Horvath-Kawazoe (H-K) and the Barret, Joyner and Halenda (BJH) methods [37–39]. The N_2 adsorption/desorption isotherms are similar for all the examined samples, calculated specific surface area is of $615 \pm 10\ m^2/g$ with pore diameter of 2.5 nm and pore volume of $0.30\ cm^3/g$ (estimated uncertainty ±5%). Time resolved photoluminescence (TR-PL) measurements were carried out in the picosecond to nanosecond time range by exciting the samples with the fs pulses generated by a kilohertz ultrafast Optical Parametric Amplifier (Spectra Physics OPA-800C). The excitation wavelength can be varied from 300 nm up to 10 μm. The OPA system is pumped with the fs pulses at 800 nm of a 1 kHz Ti:Sapphire Regenerative Amplifier System (Spectra Physics Hurricane, pulse energy > 750 microJ, pulse width < 130 fs). The signal detection was performed with a Hamamatsu streak camera (Model C5680) coupled to a EG&G spectrograph for the spectral and time resolved measurements (overall system time response shorter than 4 ps, spectral resolution 1 nm). To carry out the excitation of PL (PLE) spectra in the 400–600 nm range, the excitation light was provided by a 100 W tungsten lamp and dispersed through an Arc-Spectra-Pro 275 monochromator (excitation spectral bandwidth 2 nm). The PL spectra were recorded with a photonic multichannel analyzer (Hamamatsu PMA-11), with an emission spectral resolution of 1 nm. In order to minimize the reabsorption effects the whole set of reported measurements were performed in the "front face mode" [40], that is by recording the fluorescence signal in the backward direction, as reported in the literature for comparable systems [8–12]. Data were analyzed in the framework of the exciton theory [29,30]. The spectra were corrected for the optical transfer function of the adopted measurement system.

3. Results

The emission spectra of perchlorate samples excited at 337 nm are reported in Fig. 2: the typical PL band of Rh6G is observed,

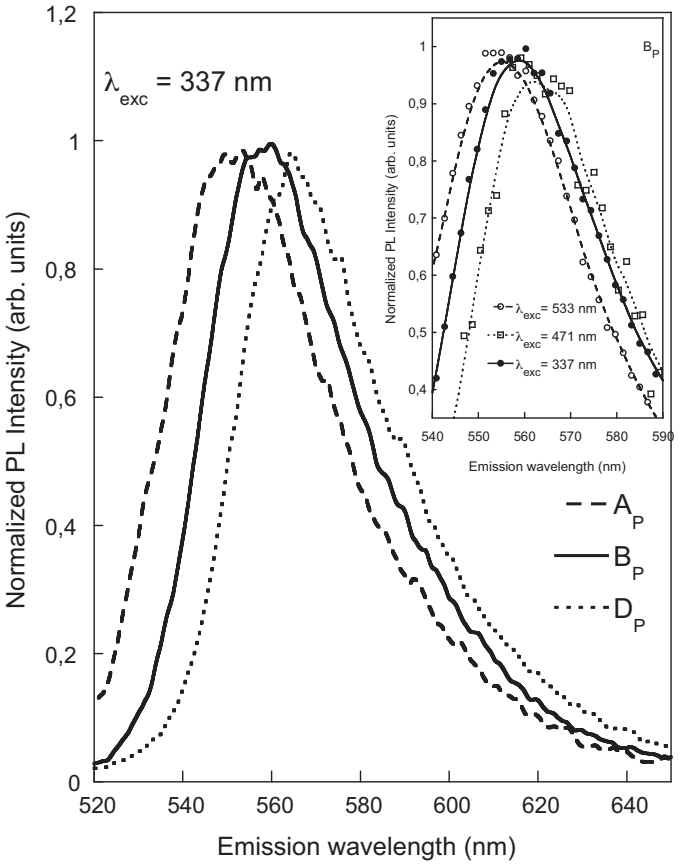

Fig. 2. PL spectra of perchlorate samples with different dye concentration ([Rh6G] = 1.6×10^{-4} mol/l in A_P, 5.2×10^{-4} mol/l in B_P, 1.6×10^{-3} mol/l in D_P) excited at 337 nm. The inset shows PL spectra of B_P samples at different excitation wavelength (solid lines are guide for the eyes).

with an emission peak at about 552 nm for the sample with lower dye concentration. By increasing the dye concentration a rigid red shift of the PL emission is observed: the peak emission red shifts up to 564 nm for the sample with the largest dye content. The spectral features (peak position and full width at half maximum, FWHM) are reported in Table 1. The inset of Fig. 2 focuses on the emission peak of the PL spectra of perchlorate B samples ([Rh6G] = 5.2×10^{-4} mol/l) excited at different excitation wavelengths (337 nm, 471 nm and 533 nm): a red shift of about 10 nm, from 555 nm to 565 nm, is detected when decreasing the excitation wavelength from 533 to 471 nm, but for the excitation at 337 nm a blue shift back to 559 nm is observed. The spectroscopic trends here reported refer to perchlorate samples but similar results also hold for chloride samples, as reported in Table 1. In Fig. 3 the analysis of the decay time of the perchlorate B samples ([Rh6G] = 5.2×10^{-4} mol/l) excited at 337 nm is reported. The typical decay time plot is reported in the inset of the figure, where the decay of the PL intensity, integrated all over the emission spectrum, is recorded as a function of the time: in general, a linear decay is observed in the semi-log plot and data were fitted with a single exponential law. Similar results also hold for the chloride samples. The results of the fitting procedure are reported in Table 1 for the whole set of samples: one can observe that the decay time increases as the dye concentration increases up to a concentration threshold ($0.5–1.0 \times 10^{-3}$ mol/l) above which it starts to decrease. The same trend is reported for the integrated area of the overall PL spectrum. In Fig. 3 the following analysis is proposed: the PL intensity of the emission band recorded by the streak camera was integrated over a small wavelength window of about 7 nm to collect the decay plot at

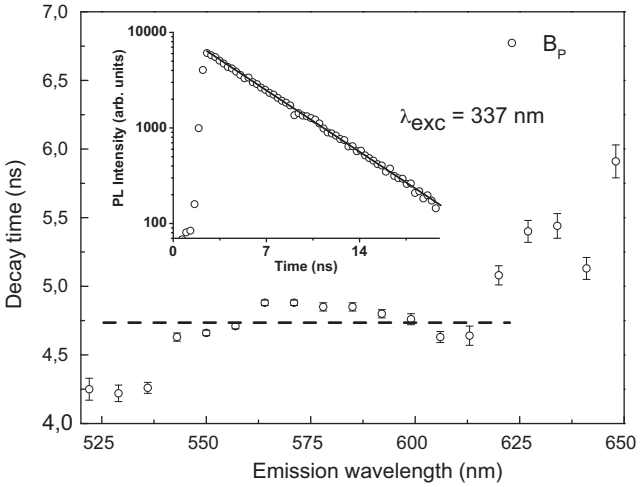

Fig. 3. Decay time of PL band at different emission wavelengths excited at 337 nm (B_P samples). The inset shows the decay plot of the integrated PL spectrum.

different emission wavelengths. The decay profiles were fitted by a single exponential law and the calculated decay times are reported as a function of the emission wavelength. In the 540–615 nm range the fitted data are scattered around the decay time value calculated for the integrated PL signal (4.75 ns, the dashed line in the figure) with deviations within the 3% (square correlation factor $R^2 > 0.96$); in the smaller (larger) wavelength region of the emission band the deviation of the calculated decay times is larger (up to 25% at 648 nm) and the fitted values are smaller (larger) than the integrated values (square correlation factor $R^2 > 0.90$). It should be kept in mind, however, that in the wings of the emission band the signal-to-noise ratio is strongly reduced, as reflected by the R^2 value. Time resolved PL spectra were also analyzed by comparing the recorded spectra at different delay from the excitation (here not shown): the PL spectrum does not undergo modifications in the spectral shape neither in the spectral position with the time after excitation.

Fig. 4 reports the PLE spectra recorded in the 400–600 nm range for two perchlorate samples (A_P with [Rh6G] = 1.6×10^{-4} mol/l, and D_P with [Rh6G] = 1.6×10^{-3} mol/l). The spectra were recorded by monitoring different emission wavelengths in the 540–620 nm range. The PLE spectrum recorded at 550 nm of a film sample, showing the typical excitation band of monomer species, is also reported for comparison [18,41]. In the smallest dye concentration case (A_P) the main excitation band is peaked at about 520 nm with a shoulder at about 490 nm when monitoring the 540 nm emission. As the monitored emission increases the main excitation channel red shifts and its bandwidth increases while the relative contribution of the 490 nm shoulder also increases. In the case of the largest dye concentration (D_P) the PLE spectrum of the emission at 540 nm is comparable to the previous one, with a main excitation band at 520 nm and a shoulder at 490 nm. As the monitored emission wavelength increases the excitation peak of the blue shoulder blue shifts down to 455 nm and its relative contribution increases up to became the main excitation band. In the meanwhile the red excitation band red shifts up to 560 nm and its bandwidth decreases; a third smaller contribution around 520 nm is also shown.

Guided by the PLE spectra, TR-PL measurements were carried out at different excitation wavelengths, namely 471 nm, 533 nm and 575 nm. The decay of the integrated PL intensity was fitted by a single exponential law. When needed a second exponential decay was added to account for the excitation light when partially overlapped to the emission band (533 and 575 nm excitations). In the case of the 575 nm excitation, data were collected in a 90° geometry, because of the large back scattered signal recorded in the front face configuration, and by using a crossed polarizer (excitation light was vertically polarized). Calculated decay times are reported in Table 2 (square correlation factor $R^2 > 0.95$). When exciting at 471 nm the emission band was merely detectable for the samples with the larger dye concentration and no attempt was performed to fit the data. In Table 2 decay times estimated under 337 nm excitation are also reported for comparison: one can see that by exciting at 575 nm the previously discussed trend of the decays is retrieved for both perchlorate and chloride samples. In the case of 533 nm excitation the monotonic trend is followed only by chloride samples while perchlorate ones show a decrease of the decay time as the dye concentration increases but for the largest dye concentration.

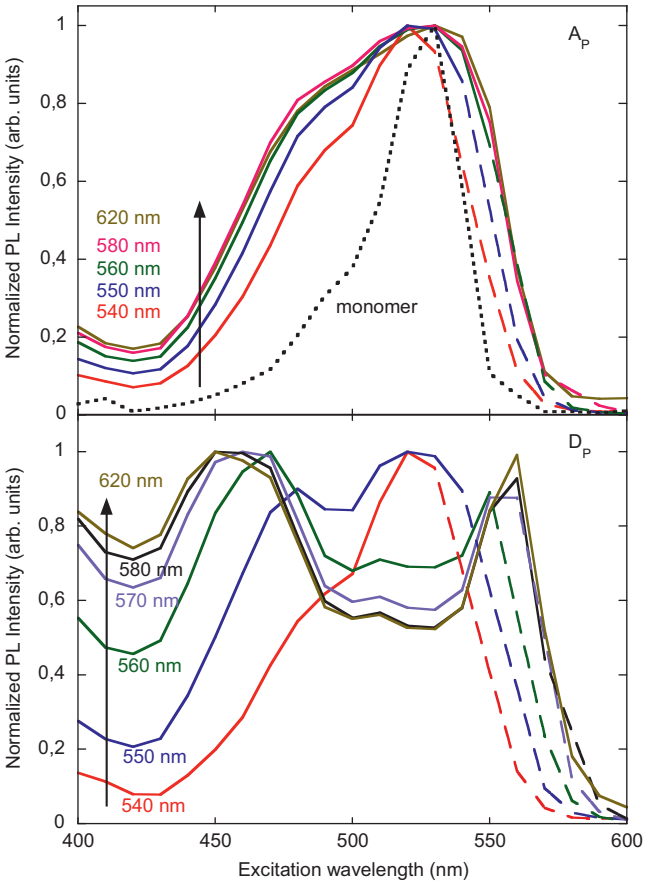

Fig. 4. PLE spectra of perchlorate samples at different dye concentration ([Rh6G] = 1.6×10^{-4} mol/l in A_P, 1.6×10^{-3} mol/l in D_P) monitored at different emission wavelengths. Dotted line: PLE spectrum of film samples recorded at 550 nm.

Table 2
Decay times of type I Rh6G–silica hybrids excited at different excitation wavelengths. "P" and "C" subscripts refer to perchlorate and chloride samples. Data between brackets refer to thermally treated samples. Decay times were estimated through a single or double exponential fit procedure applied to the integrated PL intensity, as described in the text. Estimated uncertainty was less than 0.05 ns. Square correlation factor of the fit procedure $R^2 > 0.95$.

Sample	[Rh6G] (mol/l)	λ_{exc} = 337 nm	λ_{exc} = 471 nm	λ_{exc} = 533 nm	λ_{exc} = 575 nm
A_P	1.6×10^{-4}	4.69 (4.27)	4.24	3.90	4.98
B_P	5.2×10^{-4}	4.75 (4.81)	4.52	2.99	5.13
C_P	1.0×10^{-3}	4.67 (4.74)	–	2.43	5.43
D_P	1.6×10^{-3}	3.49 (4.92)	–	2.91	5.33 (5.49)
A_C	1.6×10^{-4}	5.14 (5.06)	4.25	3.44	6.05
B_C	5.2×10^{-4}	5.21 (4.52)	3.69	3.56	6.17
C_C	1.0×10^{-3}	5.93 (5.15)	–	4.08	6.82
D_C	1.6×10^{-3}	5.22 (4.65)	–	3.34	6.41 (5.11)

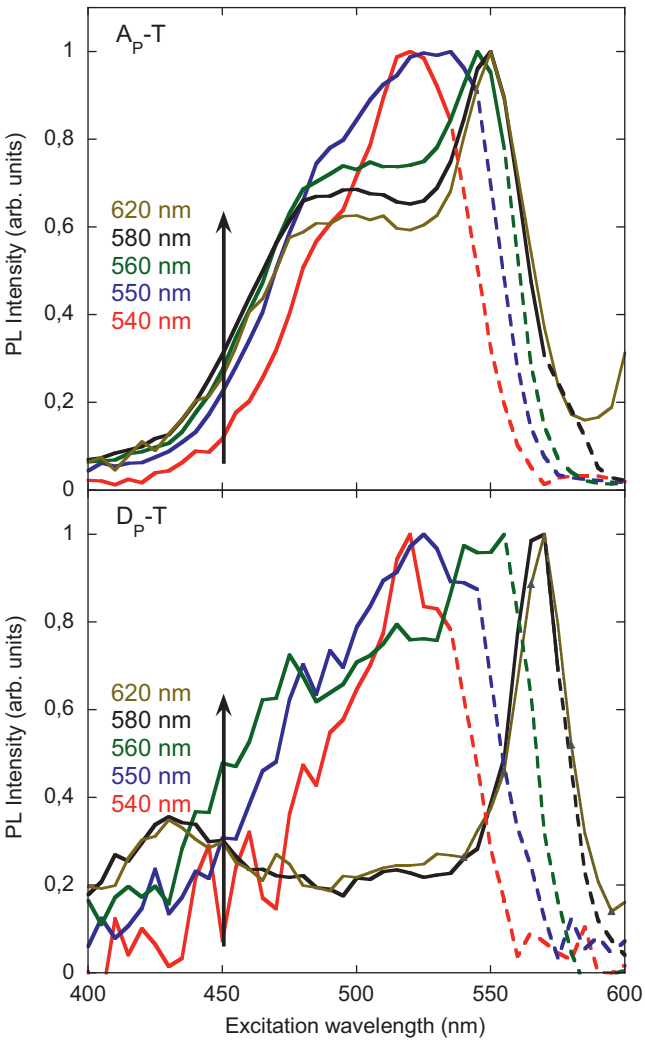

Fig. 5. PLE spectra of thermally treated perchlorate samples at different dye concentration ([Rh6G] = 1.6×10^{-4} mol/l in A_P-T, 1.6×10^{-3} mol/l in D_P-T) monitored at different emission wavelengths.

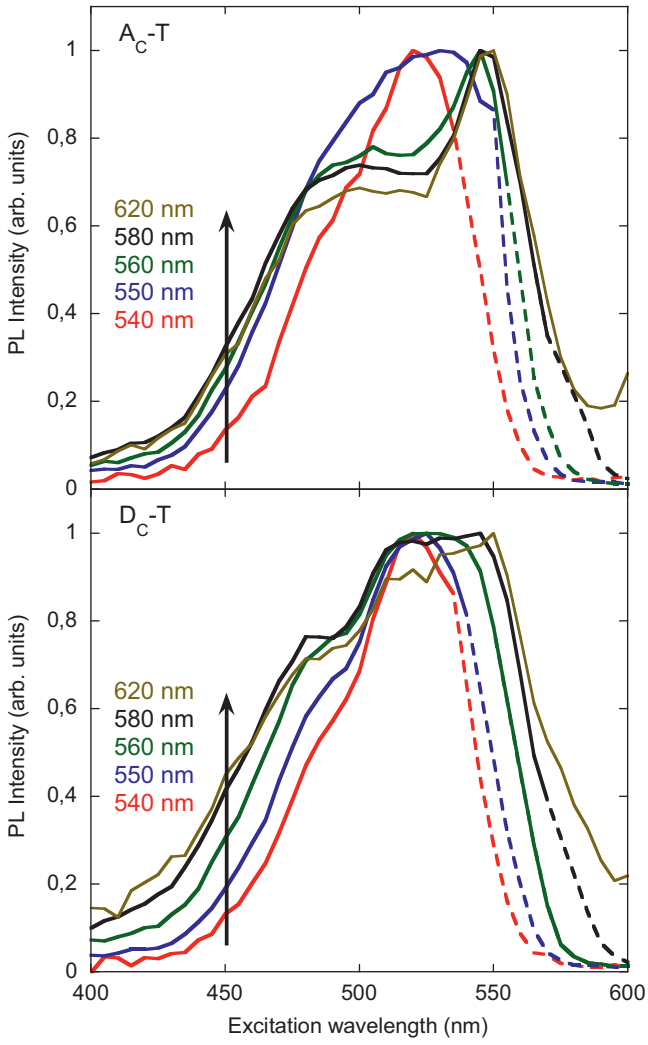

Fig. 6. PLE spectra of thermally treated chloride samples at different dye concentration ([Rh6G] = 1.6×10^{-4} mol/l in A_C-T, 1.6×10^{-3} mol/l in D_C-T) monitored at different emission wavelengths.

By comparing the estimated decay times under different excitation wavelengths at fixed dye concentration one can observe that the lifetimes decrease as the excitation wavelength increases but for the 575 nm excitation light the largest decay values are obtained. One can also compare the decay times of perchlorate and chloride samples: the latter are typically larger than the former ones, the difference being larger under 575 nm excitation.

The thermal treatment was applied to both the chloride and perchlorate samples and the emission properties of treated samples (emission peak, FWHM and decay time) are reported between brackets in Table 1. By exciting the samples at 337 nm a shift of the emission peak with respect to the peak position detected in non treated samples with the same Rh6G content was observed, in particular at the lowest dye concentrations, coupled to a slight modification of the emission decay time. However, by comparison to non treated samples, no general trends were observed in the spectral features, concerning both the peak position of the emission and the decay time.

The PLE spectra of thermally treated samples are reported in Figs. 5 and 6 in the 400–600 nm excitation range for both perchlorate and chloride samples in the case of the smaller (1.6×10^{-4} mol/l) and larger (1.6×10^{-3} mol/l) Rh6G concentration for different emission wavelengths. Regarding perchlorate samples (Fig. 5), two excitation channels are detected at about 520 and 490 nm for the 540 nm emission wavelength in both the samples. As the monitored emission wavelength increases, the bandwidth of the main excitation band increases, then a well spectrally resolved peak at about 550 nm appears and the relative contribution of the band at 490 nm decreases. In the case of the largest dye concentration the sharp excitation peak red shifts up to 570 nm and became the most intense excitation channel; at the same time the blue band blue shifts down to 440 nm and its relative contribution largely decreased. In the case of the chloride samples, the PLE spectra recorded for the sample with the smaller dye concentration are comparable to the ones of the corresponding perchlorate sample. At the largest Rh6G concentration, however, we do not observe the red shift of the peak position nor the presence of the sharp red peak: the excitation band keeps peaking at about 530 nm with an increasing bandwidth. The large change in the relative contribution and spectral resolution of the two bands reported in the perchlorate samples is not shown in the chloride case.

4. Discussion

It is well known that the Rh6G monomer specie has the main absorption peak (S_0–S_1 transition) at about 525 nm, with a vibronic shoulder around 500 nm [16]. The emission band is peaked at about 550 nm with a decay time of about 3.8 ns when hosted in

silica matrix [10] because of the reduced mobility with respect to the ethanol solution (decay time 3.0 ns [42]). A second excitation channel in the UV range (300–360 nm) is related to the S_0–S_2 transition [16]. As previously reported in comparable systems, Xanthene dyes do show aggregation phenomena when the dye concentration exceeds 4×10^{-5} mol/l [8–12]. The fluorescent properties of J dimers in Rh6G–silica samples allow to investigate and discuss their spectroscopic features in the framework of the exciton theory by recording the PL and PLE spectra and by analyzing the decay time of the recorded emissions. The present work investigate the aggregation phenomena in the concentration range around the transition threshold from fluorescent J dimers to non fluorescent H dimers, with the aim to control the aggregation phenomenon itself. Since the analyzed samples are in the 10^{-4}–10^{-3} mol/l concentration range, the recorded spectral features are ascribed to fluorescent J dimers. The shift of the PL peak emission by increasing the dye concentration or changing the excitation wavelength (Fig. 2) is a clear indication of the presence of a distribution of fluorescent J dimers [8–12,19]. This is well confirmed by the data plotted in Figs. 3 and 4: by monitoring different emission wavelengths, different excitation spectra and decay times are collected; in particular, as the emission wavelength increases the decay time increases and the split between blue and red excitation bands increases. Since the definition of the adsorption surface in porous media is non trivial, a large distribution of J dimers with slightly different spectroscopic features is indeed expected: as a consequence, the spectroscopic features reported in Table 1 should be regarded as average values [8–12,19,20]. Also the data reported in Table 2 can be interpreted in terms of a distribution of fluorescent dimers: by exciting at different excitation wavelengths we preferentially excite a specific sub-group of the distribution, thus recording the reported spectral and time variations.

A different interpretation of the reported data could also be considered: the reported data could be interpreted as the presence of different emitting species, e.g. monomers and dimers, with also the presence of possible larger aggregates. Indeed the differentiation of two or more slightly different decay times could be difficult to attempt. In this view the shift of the PL band could be ascribed to re-absorption effects due to the increasing dye concentration. However two considerations mainly lead, in our opinion, to prefer the previously proposed interpretation: first, re-absorption effects are largely reduced by the front-face geometry applied to record PL spectra [40]; second, the whole set of decay times were fitted by single exponential decays indicating the presence of a single emitting center. In addition the presence of different emitting species is also ruled out by the PL spectra recorded at different delays: the fluorescence band does not undergo spectral shifts with the time after excitation. Based on these considerations and taking into account the examined dye concentration range we propose to interpret the reported data as the spectroscopic features of a distribution of emitting J dimers.

The transition from fluorescent to non fluorescent dimers can be investigated by the analysis of time resolved PL as a function of dye concentration: when the concentration threshold is reached, non fluorescent H dimers are formed and the decrease of the recorded decay time and is expected. The same trend is expected in the value of the PL intensity. As reported in Table 1, the recorded decay time increases by increasing the Rh6G content then, above a specific dye concentration, it decreases: the decay time shortening is the signature of the increasing presence of non-radiative de-excitation pathways, such as the H dimers, that is the fingerprint of the J to H transition [8–12]. The integrated area of the PL spectrum confirmed the transition by showing the same trend. It is important to underline that the calculated decay times are intended to be mean values, since the discrimination among the contribution of different emitting species was unsuccessful: the whole set of decay times was fitted with a single exponential decay, a clear indication of a continuous distribution of aggregates with comparable average decay time, as shown in Fig. 3. The analysis was performed on the lifetimes estimated under 337 nm excitation because this excitation is within the S_0–S_2 excitation band of the monomer, which is expected to be less affected by the energy level splitting caused by the formation of dimers. In addition, the shift of the PL peak excited at 337 nm back to 559 nm, that is in between the peak position recorded under 533 and 471 nm, indicates that this wavelength is able to excite aggregates in the middle of the dimer distribution, allowing to better discuss their average spectral features. One should also note that the 337 nm wavelength corresponds to the laser line of N_2 gas laser typically used to excite Rh6G in solution, a test bed for solid state dye laser applications. The spectroscopic features reported in the analyzed spectra refer to perchlorate samples but similar results also hold for chloride samples, as reported in Table 1. However, from data listed in Table 2 one can observe that the decay time of chloride samples are larger than the ones of perchlorate samples. Larger values of lifetimes indicate that the environment sensed by the molecules is more rigid, that is a more rigid host–guest interaction: this is an indication of the role of the counterion which increases the restriction of the dye molecule mobility. This result indicate a larger reduction of the nonradiative deactivation process in chloride samples with respect to perchlorate ones, a key factor to be considered in the development of solid state dye lasers. On the contrary no variation of the spectroscopic features of emitting species, and in particular of the decay time, were recorded in ethanolic solutions of chloride and perchlorate Rh6G dyes (here not reported). On the other hand the expected differences in the aggregation phenomena due to the different tendency to dimerization of perchlorate and chloride Rh6G molecules in alcoholic solution were not observed: both perchlorate and chloride samples show the same J to H concentration threshold around $0.5–1.0 \times 10^{-3}$ mol/l. It should be kept in mind, however, that the transition from J to H dimers is not a step process but a smooth one: above the concentration threshold a large contribution of fluorescent J dimers is still recorded in the PL spectra. The contemporary presence of H and J dimers is indeed confirmed by PL spectra excited at 471 nm: the very small signal to noise ratio recorded in samples with the largest dye concentration is a clear indication of this situation, since the 471 nm band is an excitation channel of both the kind of dimers. To complete the analysis, the interpretation of the PLE spectra (Fig. 4) within the single exciton theory allows to identify the geometry of J dimers: since two excitation bands are always detected both as the monitored emission wavelength increases and as the dye concentration increases (at fixed emission wavelength) the dimers are recognized as oblique ones. The spectral modifications of the recorded PLE at different emission wavelengths (Fig. 4) is a further indication of the presence of a distribution of emitting J dimers. In order to better describe the spectral features of the dimers a Gaussian fit procedure was applied, in the energy space, to the PLE spectra recorded at different emission wavelengths. Indeed, according to the exciton theory the geometric α and R (expressed in Å) parameters (Fig. 1) of oblique fluorescent dimmers can be evaluated by means of the following equations [10,33,43]:

$$\tan^2\left(\frac{\alpha}{2}\right) = \left(\frac{A_1}{A_2}\right) \quad (1)$$

$$U = \frac{(\nu_1 - \nu_2)}{2} \quad (2)$$

$$R = \left(\frac{(1.85)10^2 \int \varepsilon_m(\nu) d\nu [\cos\alpha + 3\sin^2(\alpha/2)]}{U\nu_m}\right)^{\frac{1}{3}} \quad (3)$$

where A_1 and A_2 are the integrated area of the red and blue excitation bands of the dimers, U is the interaction energy between

Table 3
Peak position (ν_i) and energy splitting (U) of excitation bands (in cm^{-1}) as deduced by Gaussian fit procedure of PLE spectra at fixed emission wavelengths. Fitted values are also reported in nm for reference. The α and R parameters were calculated according to Eqs. (2)–(4). Data refer to AP (DP) samples ([Rh6G] = 1.6×10^{-4} mol/l and 1.6×10^{-3} mol/l respectively).

A_P (D_P)	ν_1 (cm^{-1}) λ_1 (nm)	ν_2 (cm^{-1}) λ_2 (nm)	U (cm^{-1})	α (°)	R (Å)
λ_{em} = 540 nm	18258 (18319) 548 (546)	20843 (20982) 480 (477)	1292.5 (1331.5)	42.8 (56.7)	11.9 (12.1)
λ_{em} = 550 nm	18253 (18175) 548 (550)	20988 (21303) 476 (469)	1367.5 (1564.0)	48.4 (52.6)	11.9 (11.3)
λ_{em} = 560 nm	18191 (18036) 550 (554)	21028 (21708) 476 (461)	1418.5 (1836.0)	54.9 (55.5)	11.9 (10.8)
λ_{em} = 570 nm	18194 (17980) 550 (556)	21117 (21967) 474 (455)	1461.5 (1993.5)	56.8 (56.9)	11.8 (10.5)
λ_{em} = 580 nm	18187 (17968) 550 (557)	21073 (22092) 475 (453)	1443.0 (2062.0)	54.6 (56.1)	11.8 (10.4)
λ_{em} = 620 nm	18138 (17932) 551 (558)	21069 (22162) 475 (451)	1465.5 (2115.0)	56.8 (58.9)	11.8 (10.4)

the two monomer units (in cm^{-1}), ν_m is the excitation peak of the monomers (in cm^{-1}) and $\varepsilon_m(\nu)$ is the molar absorption coefficient of the monomer band (in $M^{-1}\,cm^{-1}$). Because of the fluorescent character of the examined dimers, the analysis can be carried out on excitation spectra, as previously proposed for comparable systems [10]. On the other hand, the large absorption of the investigated samples prevented the measurement of the absorption spectrum to evaluate Eqs. (1) and (2) and the measure of the absorption spectra on comparable thick film samples [18] was not useful since in these samples aggregation effects were not observed. For this reason the PLE spectrum of a film sample (Fig. 4) was used to perform the spectral subtraction of the monomer PLE band and to obtain the excitation spectrum of dimers [10]. The results of the Gaussian fit are reported in Table 3 (peak position of the excitation bands and their spectral separation, in cm^{-1}) for two perchlorate samples (square correlation factor $R^2 > 0.95$). Beside the red and blue excitation bands picked at about 550 and 460 nm, a third excitation channel was added to account for a small shoulder at about 505 nm. From Table 3 one can observe that as the monitored emission wavelength increases the energy splitting of the blue and red excitation bands increases, the increase of the energy splitting being larger in the case of larger dye concentration (in Table 3 between brackets). By using the result of the Gaussian fit procedure and the data (ε_m and ν_m in Eq. (3)) reported in Ref. [10] the geometric parameters of the oblique dimers were calculated and reported in Table 3. As the monitored emission wavelength increases the calculated α angle for the sample with [Rh6G] = 1.6×10^{-4} mol/l increases from about 43° at 540 nm to 56° at 620 nm and the distance between monomer units keeps constant at about 12 Å, confirming the presence of a distribution of dimer aggregates with slightly different geometric parameters. In the case of [Rh6G] = 1.6×10^{-3} mol/l the α value varied around the mean value of about 56°, while the distance between monomer units decreases, from 12.1 Å at 540 nm to 10.4 Å at 620 nm. The decrease of the distance between monomer units was expected because of the larger dye concentration. One should note that the calculated distance is slightly larger than the value previously reported for comparable systems [10,12,43] or the ab initio value calculated for free standing molecules [44]. In addition the calculated α values are quite smaller than 70°, the magic angle for the formation of fluorescent aggregates [10,29,30] and the splitting between the two excitation bands is larger than the one previously reported [10]. These observations might indicate that the present interpretation based on the single exciton theory could be oversimplified and the presence of higher order of aggregates, energy transfer mechanism among different species or different geometries of the dimers, like the fluorescent twisted H-type dimers, should be also considered [22,23].

The applied thermal treatment was carried on in order to modify the contribution of different molecular species to possibly achieve a thermal tuning of specific emitting centers. It is important to underline that the applied treatment does not modify the structural and chemical properties of the dye molecule [15]. Concerning the spectral features of treated hybrids as compared to raw ones it was previously reported that the thermal treatment does not affect the PL peak position and shape when excited in the visible range [18]. The emission properties excited by UV light (Table 2) do show differences both in the peak position and decay time which can be related to a different distribution of emitting dimers. However we do not observe a monotonic red shift of the emission peak as the dye concentration increases or the monotonic variation of the decay time and PL intensity observed in the raw hybrids. The observed differences can be interpreted as the fingerprint of a different arrangement of the dye molecules at the porous surface, arrangement allowed by the applied thermal treatment. The identification of the emitting species can be carried out by the analysis of the PLE spectra in comparison to the ones of non treated samples. Few differences can be observed: at the lowest dye concentration the presence of the sharp red excitation band is observed in both perchlorate and chloride samples as the monitored emission wavelength increases, on the contrary this band was not detected in raw samples. At the largest dye concentration the thermal treatment affects in a different way perchlorate and chloride samples: in the first case the sharp red excitation band is the only excitation channel detected for emission wavelengths above 560 nm, with no sign of the red and blue bands detected in the raw samples. In the chloride case the sharp red band is merely detectable as a shoulder of the main and large red excitation band, while in raw samples its contribution was larger and well spectrally resolved. The presence of the sharp red excitation band is interpreted as the fingerprint of coplanar J dimers, showing that the aggregation can be modified by a thermal treatment up to an effective tuning of the fluorescent J dimers from oblique to coplanar ones in perchlorate samples at the largest dye concentration. Concerning the differences between perchlorate and chloride samples we can tentatively relate them to the lower tendency of the chloride Rh6G molecules to form J aggregates in alcoholic solution with respect to perchlorate samples [32]. A set of experiments on samples over a larger concentration range and dried at different temperatures up to 200° C, that is in the range of Rh6G chemical stability, is planned to elucidate the role of the drying temperature [15], the contribution of the shielding effect [28] and the one of the expected decrease of the specific surface area [45,46].

5. Conclusions

The tuning of the aggregation species in organic–inorganic hybrids is a technologically relevant issue which can be accomplished by properly engineering the synthesis of the samples. In the

case of Rh6G in porous silica matrices the dye molecules aggregate as oblique fluorescent J dimers: no differences were recorded by changing the counterion in the starting dye molecule (perchlorate or chloride Rh6G) but for a larger decrease of the dye mobility in the case of chloride samples, as deduced by the estimated decay times. The concentration limit for the transition from fluorescent J dimers to non fluorescent H dimers was estimated around 5.0×10^{-4}–1.6×10^{-3} mol/l both in the perchlorate and chloride samples. The aggregation into fluorescent dimers can be tuned from oblique to coplanar J dimers in type I hybrids by drying the samples above room temperature (at 65° C), the tuning capability depending on the dye concentration and the counterion because of the different tendency to dimerization of perchlorate and chloride samples. The formation of coplanar J dimers characterized by a very narrow excitation channel around 570 nm could offer new ranges of spectral tunability of the investigated hybrids with possible applications in the laser and optoelectronic fields.

Acknowledgment

S. Grandi, Dipartimento di Chimica Fisica, Università di Pavia (Italy) is acknowledged for the synthesis of the investigated samples. The author is grateful for the "Young Researchers" grant of the University of Cagliari.

References

[1] M. Hartmann, D. Jung, J. Mater. Chem. 20 (2010) 844–857.
[2] Y. Kim, C.-H. Kim, Y. Lee, K.-J. Kim, Chem. Mater. 22 (2010) 207–211.
[3] N.K. Mal, M. Fujiwara, Y. Tanaka, Nature 421 (2003) 350–353.
[4] G. Schulz-Ekloffa, D. Wöhrleb, B. van Duffelc, R.A. Schoonheydtc, Micropor. Mesopor. Mater. 51 (2002) 98–138.
[5] L. Malfatti, T. Kidchob, D. Aiello, R. Aiello, F. Testa, P. Innocenzi, J. Phys. Chem. C 112 (2008) 16225–16230.
[6] D. Avnir, D. Levy, R. Reisfeld, J. Phys. Chem. 88 (1984) 5956–5959.
[7] R. Reisfeld, R. Zusman, Y. Cohen, M. Eyal, Chem. Phys. Lett. 147 (1988) 142–147.
[8] F. Del Monte, D. Levy, J. Phys. Chem. B 102 (1998) 8036–8041.
[9] F. Del Monte, D. Levy, J. Phys. Chem. B 103 (1999) 8080–8086.
[10] F. Del Monte, J.D. Mackenzie, D. Levy, Langmuir 16 (2000) 7377–7382.
[11] F. Del Monte, M.L. Ferrer, D. Levy, Langmuir 17 (2001) 4812–4817.
[12] M.L. Ferrer, F. Del Monte, D. Levy, Langmuir 19 (2003) 2782–2786.
[13] A.V. Deshpande, U. Kumar, J. Lumin. 128 (2008) 1121–1131.
[14] A.V. Deshpande, U. Kumar, J. Lumin. 130 (2010) 839–844.
[15] S. Grandi, C. Tomasi, P. Mustarelli, F. Clemente, C.M. Carbonaro, J. Sol.–Gel. Sci. Technol. 41 (2007) 57–63.
[16] K.H. Drexage, Topics in Applied Physics, Springer, Berlin, 1973.
[17] A. Anedda, C.M. Carbonaro, F. Clemente, R. Corpino, S. Grandi, A. Magistris, P.C. Mustarelli, J. Non-Cryst. Solids 351 (2005) 1850–1854.
[18] C.M. Carbonaro, A. Anedda, S. Grandi, A. Magistris, J. Phys. Chem. B 110 (2006) 12932–12937.
[19] A. Anedda, C.M. Carbonaro, R. Corpino, P.C. Ricci, S. Grandi, P.C. Mustarelli, J. Non-Cryst. Solids 353 (2007) 481–485.
[20] C.M. Carbonaro, F. Meinardi, P.C. Ricci, M. Salis, A. Anedda, J. Phys. Chem. B 113 (2009) 5111–5116.
[21] Y. Lu, A. Penzkofer, Chem. Phys. 107 (1986) 175–184.
[22] F. Lopez Arbeloa, T. Lopez Arbeloa, I. Lopez Arbeloa, J. Colloid Interface Sci. 187 (1997) 105–112.
[23] V. Martınez-Martınez, F. Lopez Arbeloa, J. Banuelos Prieto, I. Lopez Arbeloa, J. Phys. Chem. B. 109 (2005) 7443–7450.
[24] V. Martınez-Martınez, F. Lopez Arbeloa, Chem. Mater. 18 (2006) 1407–1416.
[25] J. Bujdak, N. Iyi, J. Phys. Chem. B 110 (2006) 2180–2186.
[26] A. Czímerová, L. Jankovic, J. Bujdák, J. Colloid Interface Sci. 357 (2011) 322–330.
[27] V. Martınez-Martınez, C. Corcostegui, J. Banuelos Prieto, L. Gartzia, S. Salleres, I. Lopez Arbeloa, J. Mater. Chem. 21 (2011) 269–276.
[28] P. Innocenzi, H. Kozuka, T. Yoko, J. Non-Cryst. Solids 201 (1996) 26–36.
[29] E.G. McRae, M. Kasha, J. Chem. Phys. 28 (1958) 721–722.
[30] M. Kasha, H.R. Rawls, M.A. El-Bayoumi, Pure Appl. Chem. 11 (1965) 371–392.
[31] K. Kemnitz, N. Tamai, I. Yamazaki, N. Nakashima, K. Yoshihara, J. Phys. Chem. 90 (1986) 5094–5101.
[32] K. Kemnitz, K. Yoshihara, J. Phys. Chem. 95 (1991) 6095–6104.
[33] P. Bojarski, A. Matczuk, C. Bojarski, A. Kawski, B. Kuklinski, G. Zurkowska, H. Diehl, Chem. Phys. 210 (1996) 485–499.
[34] P. Bojarski, Chem. Phys. Lett. 278 (1997) 225–232.
[35] F. Lopez Arbeloa, P. Ruiz Ojeda, I. Lopez Arbeloa, J. Chem. Soc., Faraday Trans. 2 84 (1988) 1903–1912.
[36] V.V. Egorov, M.V. Alfimov, Physics-Uspekhi 50 (2007) 985–1029.
[37] S. Brunauer, P.H. Emmett, E. Teller, J. Am. Chem. Soc. 60 (1938) 309–319.
[38] G. Horvath, K. Kawazoe, J. Chem. Eng. Jpn. 16 (1983) 470–475.
[39] E.P. Barret, L.G. Joyner, P.P. Halenda, J. Am. Chem. Soc. 73 (1951) 373–380.
[40] D. Oelkrug, Topics in fluorescence spectroscopy, in: J.R. Lakowicz (Ed.), Probe Design and Chemical Sensing, vol. 4, Plenum Press, New York, 1994.
[41] To be published.
[42] M.S. Quinn, M.S. Al-Ajeel, F. Al-Bahrani, J. Lumin. 33 (1985) 53–61.
[43] M.J. Tapia Estévez, F. Lopez Arbeloa, T. Lopez Arbeloa, I. Lopez Arbeloa, R.A. Schoonheydt, Clay Miner. 29 (1994) 105–113.
[44] V.I. Gavrilenko, M.A. Noginov, J. Chem. Phys. 124, (2006) 1–6, 044301.
[45] C.J. Brinker, G.W. Schere, Sol Gel Science: The Physics and Chemistry of Sol–Gel Processing, Academic Press, San Diego, 1990.
[46] L.L. Hench, J.K. West, Chem. ReV. 90 (1990) 33.